JBC Papers in Press. Published on May 2, 2018 as Manuscript RA118.002435
The latest version is at http://www.jbc.org/cgi/doi/10.1074/jbc.RA118.002435

Structural characterization of the P^{1+} intermediate state of the P-cluster of nitrogenase

Stephen M. Keable[1]‡, Oleg A. Zadvornyy[2]‡, Lewis E. Johnson[3]‡#, Bojana Ginovska[3]‡, Andrew J. Rasmussen[4], Karamatullah Danyal[4], Brian J. Eilers[1], Gregory A. Prussia[1], Axl X. LeVan[1], Simone Raugei[2,3], Lance C. Seefeldt*[3,4], and John W. Peters*[1,2,3]

From the [1]Department of Chemistry and Biochemistry, Montana State University, Bozeman, MT 59717; [2]Institute of Biological Chemistry, Washington State University, Pullman, WA 99163; [3] Pacific Northwest National Laboratory, Richland, WA 99352; [4] Department of Chemistry and Biochemistry, Utah State University, Logan, UT 84322

Running title: *Structure of nitrogenase P-cluster intermediate*

‡ Authors made equal contributions to the paper

Present address: University of Washington, Department of Chemistry, Seattle, WA 98195;

* To whom correspondence should be addressed: John W. Peters: Institute of Biological Chemistry, Washington State University, Pullman, WA 99163, jw.peters@wsu.edu. Tel. (509) 335-3412; Lance C. Seefeldt: Department of Chemistry and Biochemistry, Utah State University, Logan, UT 84322, lance.seefeldt@usu.edu. Tel. (435) 797-3964

Keywords: redox mediators, poised states, P-cluster of MoFe protein, metalloprotein, nitrogenase, nitrogen reduction, nitrogen fixation, redox-dependent ligand exchange, [8Fe-7S] cluster

ABSTRACT

Nitrogenase is the enzyme that reduces atmospheric dinitrogen (N_2) to ammonia (NH_3) in biological systems. It catalyzes a series of single-electron transfers from the donor iron protein (Fe protein) to the molybdenum–iron protein (MoFe protein) that contains the iron-molybdenum cofactor (FeMo-co) sites where N_2 is reduced to NH_3. The [8Fe-7S] P-cluster in the MoFe protein functions in nitrogenase catalysis as an intermediate electron carrier between the external electron donor, the Fe protein, and the FeMo-co sites of the MoFe protein. Previous work has revealed that the P-cluster undergoes redox dependent structural changes and that the transition from the all-ferrous resting (P^N) state to the two electron oxidized P^{2+} state is accompanied by protein serince hydroxyl and backbone amide ligation to Fe. In this work, the MoFe protein was poised at defined potentials with redox mediators in an electrochemical cell, and the three distinct structural states of the P-cluster (P^{2+}, P^{1+}, and P^N) were characterized by X-ray crystallography and confirmed by computational analysis. These analyses revealed that the three oxidation states differ in coordination implicating that the P^{1+} state retains the serine hydroxyl coordination but lacks the backbone amide coordination observed in the P^{2+} states. These results provide a complete picture of the redox-dependent ligand rearrangements of the three P-cluster redox states.

Nitrogenase is the enzyme responsible for the multiple electron reduction of atmospheric dinitrogen (N_2) to ammonia (NH_3) in biological systems (1). This complex oxygen sensitive metalloprotein orchestrates a series of ATP-dependent single electron transfers from the donor iron protein (Fe protein) to the catalytically

active molybdenum-iron protein (MoFe protein) (2). During catalysis, the process of electron delivery to the active site involves two types of electron transfer events: one event being the intermolecular electron transfer between the [4Fe-4S] cluster of the Fe protein and the [8Fe-7S] P-clusters of the MoFe protein, and the other being the intramolecular electron transfer between the two P-clusters and two [7Fe-9S-C-Mo-homocitrate] iron-molybdenum cofactor (FeMo-co) active sites within the MoFe protein (3,4). Recent work has helped delineate the order of these electron transfer events with a proposed "deficit-spending" model (5). This model postulates that the interaction of the Fe protein and the MoFe protein elicit conformational changes that facilitate an initial “slow” and conformationally gated electron transfer step event between the P-cluster and the FeMo-co (5,6). This event leaves the P-cluster with a "deficit" of one electron, (P^{1+}) relative to the all-ferrous resting (P^N) state. This deficit is then repaid by a second, faster intermolecular electron transfer event from the reduced $[4Fe\text{-}4S]^{1+}$ cluster in the Fe protein to the P^{1+}-cluster, restoring the P^N state (5). This fast step is a direct electron transfer step and takes place at rates greater than 1700 s^{-1}, which could explain why the P^{1+} state is difficult to observe during turnover (7). Thus, the deficit spending model postulates that major conformational changes occur during catalysis, but the conformational changes that regulate the gated unidirectional electron flow are likely short-lived. The mechanistically relevant P^{1+} state has been observed spectroscopically in native and variant MoFe proteins (8-10). However, this state was only achievable using electrochemical mediators. Previous structural work has revealed two distinct conformations of the P-cluster that have been assigned to the P^N resting state and the P^{2+} oxidized state (Fig. 1) (11,12). The structures differ in the ligation of P-cluster Fe ions such that the P^{2+} oxidized state possesses two non-cysteinyl protein ligands where a serine side chain oxygen ($\beta\text{-}188^{Ser}$ according to the MoFe protein numbering from *Azotobacter vinelandii*) and a peptide backbone amide nitrogen ($\alpha\text{-}88^{Cys}$) replace two of the ligands of the hexacoordinated central sulfide present in the P^N state (Fig. 1). The P^{2+} conformation is typically seen in native MoFe protein structures due to the gradual oxidation of reductants present in the precipitant solution during crystallization. The P^N state was generated by reducing MoFe protein crystals with excess sodium dithionite just prior to flash cooling in a similar manner to the aforementioned spectroscopic studies (11,13).

The role of alternative electron transfer mechanisms involving direct oscillations between the P^N and P^{2+} states has been previously investigated (14); however various lines of evidence indicate that only single electron transfer events occur between the reduced P^N state of the P-cluster and the active site, suggesting the P^{1+}/P^N couple is the predominant oscillation of the P-cluster under turnover conditions (15). The P^N and P^{2+} states are structurally accessible and provide fascinating insights implicating redox dependent structural changes in the nitrogenase mechanism, but completing the understanding of the mechanistic cycle requires knowledge of the structure of the catalytically relevant P^{1+} state. To elucidate the structure of the P^{1+} state, structures of the nitrogenase MoFe protein were solved for crystals poised at defined oxidation-reduction potentials with redox mediator solutions in an electrochemical cell. In addition, computational analysis has been performed to evaluate the ligation of P-cluster by $\alpha\text{-}88^{Cys}$ and $\beta\text{-}188^{Ser}$ side chains corresponding to three ($P^{2+}/P^{1+}/P^N$) oxidation states of P-cluster observed for MoFe protein. Together the results reveal a new state of the P-cluster with coordination distinct from the previously characterized P^{2+} and P^N oxidation states.

Results

Crystals of MoFe protein were poised at different potentials in an electrochemical cell containing mother liquor supplemented with redox active dyes (Fig. 2). Constant stirring maintained a homogenous charge throughout the solution, and a “sandwich-loop” crystal mounting technique was developed to prevent the crystals from washing off the loop during electrochemical poising. After 1h of incubation in the electrochemical cell at known potential the nitrogenase crystals were flash frozen in liquid nitrogen. The poised crystals in the presence of redox mediators were highly sensitive to x-rays regardless of potential through the range of

poised samples. The plate morphology of the crystals prevented collecting complete data sets in all cases due to the extremely rapid decay observed when data collection was attempted across the long angle of the crystals. Despite being only able to obtain partial data sets (~60%), it was possible to reproduce our previously published results and confirm structural differences between P^N and P^{2+} states (Table S1, and S2). Crystals of MoFe protein treated with flavin mononucleotide and held at -238 mV revealed a novel intermediate structure distinct from the P^N and P^{2+} structures in ligation, which was assigned as the P^{1+} state. Feature-enhanced electron density maps (16) were of sufficient quality to clearly distinguish the observed intermediate P-cluster structural state from the previously reported P-cluster P^N and P^{2+} structures (Fig. 3 and Table S2). The structural differences observed in comparing the assigned P^N, P^{1+}, and P^{2+} oxidation states are manifested solely in changes in cluster ligation. Interestingly, the new state, assigned as the P^{1+} state, was only observed on one αβ dimer of the 2-fold symmetric $\alpha_2\beta_2$ heterotetrameric MoFe protein, the P-cluster in the second αβ dimer was found to be in P^{2+} oxidation state. The P^{1+} state structure has a ligand arrangement intermediate between the P^N and P^{2+} states. The P^{1+} state possesses serine coordination to Fe, but lacks the amide nitrogen ligation seen in the P^{2+} state. *Fo-Fc* difference density analysis experiments were carried out between the P^{1+} and P^N, P^{1+} and P^{2+}, and the P^N and P^{2+} structures to provide additional support for the new structural state. (Fig. 4). The observation that the amide nitrogen ligand is exchanged by ligation to the central S prior to the serine oxygen coordination in the redox progression during reduction can be rationalized from the perspective of the hard/soft and acid/base (HSAB) theory since nitrogen is a slightly harder and weaker ligand than oxygen and its affinity would be further decreased on reduction of the metal to be ligated. Thus, the suite of P-cluster structures provides evidence to suggest that the first oxidizing equivalent changes the structure of the Fe atom near the β-188^{Ser} and may oxidize this Fe first. The second oxidizing equivalent would then oxidize the Fe atom near the α-88^{Cys}.

Density functional theory (DFT) calculations were performed for the three oxidation states of the P-cluster in order to evaluate the relative sequence of binding of the serine and amide ligands. The energy ordering of the possible ligation forms for every given oxidation state is reported in Fig. 6. Consistent with the experimental evidence, in the lowest-energy P^N state structure both α-88^{Cys} and β-188^{Ser} are not bound. The α-88^{Cys}, P^N_C, and β-188^{Ser} P^N, P^N_S, ligated are only 9 kJ/mol and 11 kJ/mol higher in energy than the non-ligated P-cluster form, P^N. In stark contrast, the doubly ligated, P^N_{SC}, isomer is 174 kJ/mol above the non-ligated P^N form. Oxidation of P^N by one or two electrons dramatically alters the ligation preference of the cluster. The β-188^{Ser} ligated state, P^{1+}_S, is calculated to be the most stable one-electron oxidized form of the P-cluster, -4 kJ/mol lower in energy than the non-ligated form, while the α-88^{Cys} ligated form, P^{1+}_C, and doubly ligated P^{1+}_{SC} form are far higher in energy. Double oxidation of the P-cluster (P^{2+}) favors binding of both α-88^{Cys} and β-188^{Ser}, with the double ligated P^{2+}_{SC} being significantly more stable then P^{2+}_C state, by 55 kJ/mol, and only slightly less stable, by 2 kJ/mol, then P^{2+}_S. When more accurate treatment of the zero-point correction is employed, the order of the P^{2+}_S and P^{2+}_{SC} inverts, with P^{2+}_{SC} being more stable by 37 kJ/mol (Figure S2). Unfortunately, due to numerical issues, this approach was not available for all states.

Taken as a whole, these calculations confirm that the serine side chain has a higher binding affinity than the Cys backbone amide nitrogen, and that the serine side chain preferentially binds to the P-cluster after the first oxidation event (P^{1+}), while double oxidation (P^{2+}) greatly increases the binding affinities resulting in the preferential formation of the doubly-ligated form of the P-cluster.

Discussion

This newly visualized P^{1+} state is compatible with the proposed deficit spending mechanism and demonstrates a redox-mediated ligand exchange mechanism for possibly regulating electron flow for the P^{1+}/P^N redox couple. Previous mutagenesis studies targeting the β-188^{Ser} P-cluster ligand have utilized the introduction of a stronger ligand, such as cysteine,

or removal of coordination by glycine substitution to stabilize the P-cluster in the P^{1+} and P^N states by shifting the resting potential of the cluster -90 mV and +60 mV, respectively (4,17). Interestingly, these amino acid substitutions confer lower specific activities to the variants by disrupting a key exchangeable ligand (4,5). These observations add support to our P^{1+} assignment of this structure and the prominence of a ligand exchange mechanism in nitrogenase catalysis. Recently, we have shown that amino acid substitutions near the proximal side of the P-cluster cubane relative to FeMo-co (Fe1-4 based on the PDB numbering scheme), such as β-98$^{Tyr→His}$, β-99$^{Phe→His}$, and α-64$^{Tyr→-His}$, generate protein variants that are capable of being reduced by low reduction potential mediators which have Eu(II) ligated to polyaminocarboxylate ligands, while substitutions near the Fe 5-8 cubane (distal to side to FeMo-co) do not show this behavior (18,19). Analyzing this information in light of our current finding, we can assign directional character to the P-cluster. Here based on the substitution studies, the proximal side of the cubane relative to FeMo-co would be involved in the electron transfer between the P-cluster and FeMo-co during the slow step, while the distal cubane undergoes structural conformational changes in order to accommodate the loss of an electron from the P-cluster (Fig. 5).

We have also recently shown that electron transfer between the Fe protein and the MoFe protein precedes ATP hydrolysis (20). Conformational changes within the P-cluster of the MoFe protein during the deficit spending events could potentially serve as triggers for the initiation of the ATP hydrolysis step within the Fe protein. This would result in the Fe protein cycle of electron transfer being a conformationally controlled series of events. Furthermore, it has been previously suggested that the Fe protein – MoFe protein interaction could cause the β-188^{Ser} to transiently coordinate to the P-cluster, creating an activated P-cluster state (designated P^N_S) with a lowering of the potential to facilitate electron transfer between the P-cluster and FeMo-cofactor (5). Consistent with this hypothesis, the present DFT calculations predict the ligated P^N_S state only 9 kJ/mol higher in energy than the P^N state, and therefore potentially accessible upon slight distortion of the P-cluster environment.

The one-electron ligand exchange also raises the possibility of the involvement of the P-cluster in a proposed proton coupled electron transfer (PCET) mechanism in nitrogenase. The β-188^{Ser} hydroxyl and α-88^{Cys} amide would presumably be protonated when not coordinated to the P-cluster. Potential proton donor/acceptors are within hydrogen bonding distance of the β-188^{Ser} hydroxyl group (an ordered water molecule) and the α-88^{Cys} backbone amide (α-153^{Glu} side chain). Sequential hydride formation has been postulated as part of the catalytic cycle (21), therefore the single redox P^{1+}/P^N couple fits well into the most recent proposed deficit spending mechanism. Additionally, previous spectroscopic studies have also shown residues around the distal side of the P-cluster cubane (relative to FeMo-co) to be involved in PCET (17). Although this unique iron-sulfur cluster has been shown to undergo unprecedented redox-mediated structural changes, a complete understanding of the unidirectional PCET is difficult without more information regarding the complex and dynamic global conformational changes that occur when the Fe protein interacts with the MoFe protein. Current structural techniques have failed to provide details of these transient global conformational changes. By utilizing a new redox crystallography approach, complemented by DFT calculations, we are now able to populate some of these difficult to obtain transient states and piece together the details of one of nature's most enigmatic catalytic cycles. The work presented here also has relevance to probing electron flow and redox mediated structural changes in numerous metalloprotein systems, providing possible insights into biological electron transfer

Experimental procedures

Purification and crystallization of MoFe protein. All chemicals were purchased from Sigma-Aldrich (St. Louis, MO) or Fischer Scientific (Fair Lawn, NJ) and were used without further purification. Wild type MoFe protein from *Azotobacter vinelandii* was purified under strict anaerobic conditions according to previously described protocols (22). All proteins were obtained at greater than 95% purity and

confirmed by SDS-PAGE analysis using Coomassie blue staining and demonstrated maximal specific activity (greater than 2,000 nmol H_2/min/mg MoFe protein). Handling of proteins was done in septum-sealed serum vials under an argon atmosphere. All transfer of gases and liquids were done using gastight syringes. Protein crystals were grown by capillary batch diffusion in a 100% N_2 atmosphere MBraun glove box with previously reported precipitant solutions (23).

Poising crystals of FeMo protein with redox mediators. Crystals were harvested anaerobically under an argon stream and immobilized on pins using a novel "sandwich" loop designed to prevent the crystals from washing away during electrochemical studies. Two micromesh loops (MiTiGen LLC, Ithaca, NY) were affixed on top of each other to the same pin, and a small piece of monofilament was placed in between to separate them. Crystals were positioned between the loops, and the monofilament was then removed to apply tension from the loops to secure the crystals. The immobilized crystals were immediately submerged in an electrode solution mimicking the precipitant solution composed of 18% PEG 4000, 50 mM Tris-HCl buffer pH 8.0, 15% glycerol, 100 mM sodium chloride, and 1 mM of a redox mediator. The mediators used were methylene blue, flavin mononucleotide, and methyl viologen with midpoint potentials (E_m) of +11mV, -238 mV, and -488 mV respectively vs. standard hydrogen electrode (24). The mediator solutions were degassed and placed in an electrochemical cell with a built-in graphite working electrode (2.8 cm^2 surface area), a mesh platinum counter electrode separated by a vycor conductive glass plug, and a saturated calomel electrode (SCE) reference electrode (Fig. 2). The solutions were kept under a constant stream of humidified argon to maintain anaerobicity without modifying solution volume. The electrode solutions were poised at +11mV, -238 mV, and -488 mV vs. normal hydrogen electrode (NHE) for methylene blue, flavin mononucleotide, and methyl viologen, respectively. An OMNI-101 microprocessor controlled potentiostat (Cypress Systems, Lawrence, Kansas) was used to control potential and constant stirring was used to achieve a uniform solution. The submerged sandwich looped crystals were allowed to soak for 1 hour and were immediately flash cooled in liquid nitrogen to preserve the poised states.

Data collection and refinement. Data was collected at SSRL BL12-2 for native *A. vinelandii* MoFe protein poised at three defined potentials. Due to the increased susceptibility to radiation damage caused by the mediator solution treatment, only partial data sets could be collected. Processed data completeness (~60%) and resolution (~2.2 Å) was similar for the poised data sets (Table 1, Table S1, S2) (25). The previously determined MoFe protein structure P^{2+} state (PDB 2MIN) was used as a starting for refinement (26-29). The P^{1+} structure has been deposited in the Protein Data Bank as entry 6CDK. Feature-enhanced electron density map (FEM) was calculated using phinex.fem (16). Difference electron density maps were calculated using Phenix (26) and CCP4 (29) program suites.

Computational methods. Electronic structure calculations of the structure and energetics of different states of the P-cluster, were performed based on broken symmetry DFT. The DFT model includes the P-cluster, all residues covalently bonded to the cluster, all residues with protic hydrogens within hydrogen bonding distance of the P-cluster, and all waters within hydrogen bonding distance of any of the above. Residues were truncated at the β-carbon and hydrogen-terminated unless the backbone participated in any included hydrogen bonding interactions. When backbones were retained, the backbones were methyl-terminated beyond the included residues. The QM structure was taken from a representative configuration of the enzyme generated as obtained from molecular dynamics (MD) simulations of the nitrogenase complex. Details about the MD simulation and electronic structure methods are included as SI. The structures were optimized in gas phase keeping the position of the C atoms of the residues that were truncated frozen (Fig S1 in SI). Calculations were performed with the NWChem (30) 6.6 quantum chemistry package using both the BP86 exchange and correlation functional (31,32) and, for select structures, the B3LYP hybrid functional (33). The calculations adopted the following basis set: Ahlrichs (34) VTZ for Fe, 6-311++G** (35,36) for the atoms coordinated to

the Fe atoms or belonging to moieties engaging direct hydrogen-bonds with the P cluster, instead the 6-31G* (37) was adopted for all other atoms (Fig S1 in SI). The effect of the protein environment beyond the outer coordination sphere of the P-cluster explicitly included in the calculation was modeled as a dielectric continuum using the COnductor-like Screening MOdel (COSMO) framework using a dielectric constant of 10 (38,39). Due to numerical instabilities in the vibrational analysis for some states, we were only able to obtain reliable zero-point correction for 8 of the considered 12 states using normal mode analysis performed within the rigid rotor-harmonic approximation, after projecting out spurious imaginary frequencies arising from the positional constrains in the geometries. For this reason, we used an approximation where we correct for the energy of the vibrational mode associated with the lost –OH (41.5 kJ/mol) or –NH bond (40.5 kJ/mol). We benchmarked this approximation against the calculated full zero-point correction energy for the states for which reliable frequencies were available, and found it to provide excellent results (table S4 and figure S2 in the SI). Absolute values for the gas phase and solvent phase energies, as well as zero-point corrections are provided in table S4. The relative ordering of states was also conserved if geometries were optimized using the B3LYP hybrid functional (table S5). In the following, we discuss the BP86 energies only since this functional yields geometries for P^N and P^{2+}_{SC} states that are in far better agreement with the crystallographic data than those produced using the B3LYP functional, as reported in table S5 of the SI.

Calculations were performed on all the three oxidation states of the P-cluster (P^N, P^{2+}, P^{1+}) with and without the Ser -OH and Cys backbone bound. For the reduced state, P^N, Mossbauer studies (9) have shown that all Fe atoms are in the +2 state, antiferromagnetically coupled for an overall $S = 0$ spin. The present calculations reproduce this experimental observation, predicting the $S = 0$ being the most stable (Table S3). As for the P^{1+} state, our calculation clearly indicate that it is a doublet ($S = 1/2$), while the P^{2+} state is a singlet. More details about the stability of the different oxidation states are provided in the Supporting information (table S7).

Ligation of Ser and Cys backbone require their deprotonation, which implies the knowledge of the pK_a values of these residues, and in turn the free energy of the solvated proton in water. High accuracy extrapolations of the latter are available(40) but their use is problematic because of inconsistencies between the level of theory adopted in the present calculations and those adopted for the extrapolation. Therefore, we avoided the direct use of the free energy of the solvated proton by estimating the overall energetics of ligation for each oxidation state of the P-cluster with respect to methanol (Ser ligation) and methylacetamide (Cys backbone amide) in aqueous solution, of which accurate pK_a values are available. Details of the calculation are provided in the SI.

Acknowledgments: This work was supported by a grant from the National Science Foundation (MCB-1330807) to J.W.P and L.C.S., and from U.S. Department of Energy (DOE), Office of Science, Basic Energy Sciences (BES), Division of Chemical Sciences, Geosciences, and Biosciences under contract DE-AC05-76RL01830 to L.E.J., B.G. and S.R. Use of the Stanford Synchrotron Radiation Lightsource, SLAC National Accelerator Laboratory, is supported by the U.S. DOE, Office of Science, BES under Contract DE-AC02-76SF00515. The SSRL Structural Molecular Biology Program is supported by the DOE Office of Biological and Environmental Research and by the National Institutes of Health, National Institute of General Medical Sciences (including Grant P41GM103393). Computer resources were provided by the W. R. Wiley Environmental Molecular Sciences Laboratory (EMSL), a DOE Office of Science User Facility located at Pacific Northwest National Laboratory and sponsored by DOE's Office of Biological and Environmental Research.

Conflict of interest: The authors declare that they have no conflict of interest with the contents of this article.

Author contributions: SMK, OAZ, LEJ and BG made equal contributions to the paper. SMK, SR, LCS, JWP designed the experiments. SMK, AJR, KD, GAP, AXL performed potentiometric titration of the nitrogenase crystals. SMK, OAZ, BJE, AXL collected and analyzed X-ray data. LEJ, BG and SR performed the simulations and analyzed corresponding results. SMK, OAZ, LEJ, BG, JWP wrote the paper with LCS and SR.

FOOTNOTES

The abbreviations used are: P-cluster, [8Fe-7S] cluster of MoFe protein; MoFe protein, Molybdenum-iron protein of nitrogenase; Fe protein, Iron protein of nitrogenase; FeMo-co, [7Fe-9S-C-Mo-homocitrate] iron-molybdenum cofactor; COSMO, Conductor-like screening model; PCET, Proton Coupled Electron Transfer; QM, Quantum mechanics; MD, Molecular Dynamics; BP86, Becke exchange and Perdew correlation functional; B3LYP hybrid functional, Becke Lee Yang Parr hybrid functional.

References

1. Burgess, B. K., and Lowe, D. J. (1996) Mechanism of Molybdenum Nitrogenase. *Chemical Reviews* **96**, 2983-3012
2. J B Howard, a., and Rees, D. C. (1994) Nitrogenase: A Nucleotide-Dependent Molecular Switch. *Annual Review of Biochemistry* **63**, 235-264
3. Hageman, R. V., and Burris, R. H. (1978) Nitrogenase and nitrogenase reductase associate and dissociate with each catalytic cycle. *Proceedings of the National Academy of Sciences* **75**, 2699-2702
4. Chan, J. M., Christiansen, J., Dean, D. R., and Seefeldt, L. C. (1999) Spectroscopic evidence for changes in the redox state of the nitrogenase P-cluster during turnover. *Biochemistry* **38**, 5779-5785
5. Danyal, K., Dean, D. R., Hoffman, B. M., and Seefeldt, L. C. (2011) Electron transfer within nitrogenase: evidence for a deficit-spending mechanism. *Biochemistry* **50**, 9255-9263
6. Tezcan, F. A., Kaiser, J. T., Mustafi, D., Walton, M. Y., Howard, J. B., and Rees, D. C. (2005) Nitrogenase Complexes: Multiple Docking Sites for a Nucleotide Switch Protein. *Science* **309**, 1377-1380
7. Lowe, D. J., Fisher, K., and Thorneley, R. N. F. (1993) Klebsiella pneumoniae nitrogenase: pre-steady-state absorbance changes show that redox changes occur in the MoFe protein that depend on substrate and component protein ratio; a role for P-centres in reducing dinitrogen? *Biochemical Journal* **292**, 93-98
8. Yoo, S. J., Angove, H. C., Papaefthymiou, V., Burgess, B. K., and Münck, E. (2000) Mössbauer Study of the MoFe Protein of Nitrogenase from Azotobacter vinelandii Using Selective 57Fe Enrichment of the M-Centers. *Journal of the American Chemical Society* **122**, 4926-4936
9. Lindahl, P. A., Papaefthymiou, V., Orme-Johnson, W. H., and Münck, E. (1988) Mössbauer studies of solid thionin-oxidized MoFe protein of nitrogenase. *Journal of Biological Chemistry* **263**, 19412-19418
10. Rupnik, K., Hu, Y., Lee, C. C., Wiig, J. A., Ribbe, M. W., and Hales, B. J. (2012) P+ state of nitrogenase p-cluster exhibits electronic structure of a [Fe4S4]+ cluster. *J Am Chem Soc* **134**, 13749-13754
11. Peters, J. W., Stowell, M. H., Soltis, S. M., Finnegan, M. G., Johnson, M. K., and Rees, D. C. (1997) Redox-dependent structural changes in the nitrogenase P-cluster. *Biochemistry* **36**, 1181-1187
12. Chan, M. K., Kim, J., and Rees, D. (1993) Pair: 2.2 A Resolution Structures. *Science* **260**, 7
13. Tittsworth, R. C., and Hales, B. J. (1993) Detection of EPR signals assigned to the 1-equiv-oxidized P-clusters of the nitrogenase MoFe-protein from Azotobacter vinelandii. *Journal of the American Chemical Society* **115**, 9763-9767
14. Lowery, T. J., Wilson, P. E., Zhang, B., Bunker, J., Harrison, R. G., Nyborg, A. C., Thiriot, D., and Watt, G. D. (2006) Flavodoxin hydroquinone reduces Azotobacter vinelandii Fe protein to the all-ferrous redox state with a S = 0 spin state. *Proceedings of the National Academy of Sciences* **103**, 17131-17136
15. Seefeldt, L. C., Hoffman, B. M., and Dean, D. R. (2009) Mechanism of Mo-dependent nitrogenase. *The Annual Review of Biochemistry* **78**, 701-722

16. Afonine, P. V., Moriarty, N. W., Mustyakimov, M., Sobolev, O. V., Terwilliger, T. C., Turk, D., Urzhumtsev, A., and Adams, P. D. (2015) FEM: feature-enhanced map. *Acta Crystallogr D Biol Crystallogr* **71**, 646-666
17. Lanzilotta, W. N., Christiansen, J., Dean, D. R., and Seefeldt, L. C. (1998) Evidence for coupled electron and proton transfer in the [8Fe-7S] cluster of nitrogenase. *Biochemistry* **37**, 11376-11384
18. Danyal, K., Inglet, B. S., Vincent, K. A., Barney, B. M., Hoffman, B. M., Armstrong, F. A., Dean, D. R., and Seefeldt, L. C. (2010) Uncoupling nitrogenase: catalytic reduction of hydrazine to ammonia by a MoFe protein in the absence of Fe protein-ATP. *Journal of the American Chemical Society* **132**, 13197-13199
19. Danyal, K., Rasmussen, A. J., Keable, S. M., Inglet, B. S., Shaw, S., Zadvornyy, O. A., Duval, S., Dean, D. R., Raugei, S., and Peters, J. W. (2015) Fe Protein-Independent Substrate Reduction by Nitrogenase MoFe Protein Variants. *Biochemistry* **54**, 2456-2462
20. Duval, S., Danyal, K., Shaw, S., Lytle, A. K., Dean, D. R., Hoffman, B. M., Antony, E., and Seefeldt, L. C. (2013) Electron transfer precedes ATP hydrolysis during nitrogenase catalysis. *Proceedings of the National Academy of Sciences of the United States of America* **110**, 16414-16419
21. Yang, Z. Y., Danyal, K., and Seefeldt, L. C. (2011) Mechanism of Mo-dependent nitrogenase. *Methods in Molecular Biology* **766**, 9-29
22. Burgess, B. K., Jacobs, D. B., and Stiefel, E. I. (1980) Large-scale purification of high activity Azotobacter vinelandii nitrogenase. *Biochimica et Biophysica Acta (BBA)-Enzymology* **614**, 196-209
23. Sarma, R., Barney, B. M., Keable, S., Dean, D. R., Seefeldt, L. C., and Peters, J. W. (2010) Insights into substrate binding at FeMo-cofactor in nitrogenase from the structure of an alpha-70(Ile) MoFe protein variant. *Journal of Inorganic Biochemistry* **104**, 385-389
24. Lanzilotta, W. N., and Seefeldt, L. C. (1997) Changes in the midpoint potentials of the nitrogenase metal centers as a result of iron protein-molybdenum-iron protein complex formation. *Biochemistry* **36**, 12976-12983
25. Otwinowski, Z., and Minor, W. (1997) Processing of X-ray diffraction data collected in oscillation mode. *Methods Enzymol* **276**, 307-326
26. Adams, P. D., Afonine, P. V., Bunkoczi, G., Chen, V. B., Davis, I. W., Echols, N., Headd, J. J., Hung, L. W., Kapral, G. J., Grosse-Kunstleve, R. W., McCoy, A. J., Moriarty, N. W., Oeffner, R., Read, R. J., Richardson, D. C., Richardson, J. S., Terwilliger, T. C., and Zwart, P. H. (2010) PHENIX: a comprehensive Python-based system for macromolecular structure solution. *Acta Crystallogr D Biol Crystallogr* **66**, 213-221
27. Afonine, P. V., Grosse-Kunstleve, R. W., Echols, N., Headd, J. J., Moriarty, N. W., Mustyakimov, M., Terwilliger, T. C., Urzhumtsev, A., Zwart, P. H., and Adams, P. D. (2012) Towards automated crystallographic structure refinement with phenix.refine. *Acta Crystallogr D Biol Crystallogr* **68**, 352-367
28. Murshudov, G. N., Vagin, A. A., and Dodson, E. J. (1997) Refinement of macromolecular structures by the maximum-likelihood method. *Acta Crystallogr D Biol Crystallogr* **53**, 240-255
29. Winn, M. D., Ballard, C. C., Cowtan, K. D., Dodson, E. J., Emsley, P., Evans, P. R., Keegan, R. M., Krissinel, E. B., Leslie, A. G., McCoy, A., McNicholas, S. J., Murshudov, G. N., Pannu, N. S., Potterton, E. A., Powell, H. R., Read, R. J., Vagin, A., and Wilson, K. S.

(2011) Overview of the CCP4 suite and current developments. *Acta Crystallogr D Biol Crystallogr* **67**, 235-242

30. Valiev, M., Bylaska, E. J., Govind, N., Kowalski, K., Straatsma, T. P., Van Dam, H. J. J., Wang, D., Nieplocha, J., Apra, E., Windus, T. L., and de Jong, W. A. (2010) NWChem: A comprehensive and scalable open-source solution for large scale molecular simulations. *Computer Physics Communications* **181**, 1477-1489
31. Perdew, J. P. (1986) Density-functional approximation for the correlation energy of the inhomogeneous electron gas. *Phys. Rev. B* **33**, 8822-8824
32. Becke, A. D. (1988) Density-functional exchange-energy approximation with correct asymptotic behavior. *Phys. Rev. A* **38**, 3098-3100
33. Stephens, P. J., Devlin, F. J., Chabalowski, C. F., and Frisch, M. J. (1994) Ab Initio Calculation of Vibrational Absorption and Circular Dichroism Spectra Using Density Functional Force Fields. *The Journal of Physical Chemistry* **98**, 11623-11627
34. Schäfer, A., Huber, C., and Ahlrichs, R. (1994) Fully optimized contracted Gaussian basis sets of triple zeta valence quality for atoms Li to Kr. *The Journal of Chemical Physics* **100**, 5829-5835
35. Krishnan, R., Binkley, J. S., Seeger, R., and Pople, J. A. (1980) Self‐consistent molecular orbital methods. XX. A basis set for correlated wave functions. *The Journal of Chemical Physics* **72**, 650-654
36. Clark, T., Chandrasekhar, J., Spitznagel, G. n. W., and Schleyer, P. V. R. (1983) Efficient diffuse function-augmented basis sets for anion calculations. III. The 3-21+G basis set for first-row elements, Li-F. *Journal of Computational Chemistry* **4**, 294-301
37. Hehre, W. J., Ditchfield, R., and Pople, J. A. (1972) Self—Consistent Molecular Orbital Methods. XII. Further Extensions of Gaussian—Type Basis Sets for Use in Molecular Orbital Studies of Organic Molecules. *The Journal of Chemical Physics* **56**, 2257-2261
38. Pitera, J. W., Falta, M., and van Gunsteren, W. F. (2001) Dielectric properties of proteins from simulation: the effects of solvent, ligands, pH, and temperature. *Biophys J* **80**, 2546-2555
39. Li, L., Li, C., Zhang, Z., and Alexov, E. (2013) On the Dielectric "Constant" of Proteins: Smooth Dielectric Function for Macromolecular Modeling and Its Implementation in DelPhi. *Journal of Chemical Theory and Computation* **9**, 2126-2136
40. Kelly, C. P., Cramer, C. J., and Truhlar, D. G. (2006) Aqueous solvation free energies of ions and ion-water clusters based on an accurate value for the absolute aqueous solvation free energy of the proton. *J Phys Chem B* **110**, 16066-16081

Table 1. Data collection and refinement statistics for P^{1+} dataset.

Data Statistics	P^{1+} dataset
Cell dimensions	a = 80.79 Å b = 130.78 Å c = 107.88 Å α = γ = 90.00° β = 110.85
Space group	P21
Wavelength	λ1 = 0.97947
Resolution (Å)	50-2.10
Completeness (%)	57.06 (60.8)a
Obsd reflections	150869
Unique reflections	70560
Avg redundancy	2.1
I/σ	4.0 (1.3)a
Rsym (%)	14.2 (54.4) a
CC (1/2)	0.992 (0.814)a
Refinement Statistics for P^{+1}	
Resolution (Å)	50-2.1
Rcyrstc (%)	23.2
Rfreec (%)	26.3
Real Space CCd (%)	
Mean B Value (overall; Å)	24.5
Coordinate Error (based on maximum likelihood, Å)	0.22
RMSD from ideality:	
Bonds (Å)	0.018
Angles (°)	2.291
Ramchandran Plot	
Most favored (%)	95.08
Additional allowed (%)	4.67
Outliers (%)	0.25

[a] Numbers in parenthesis refer to the highest resolution shell

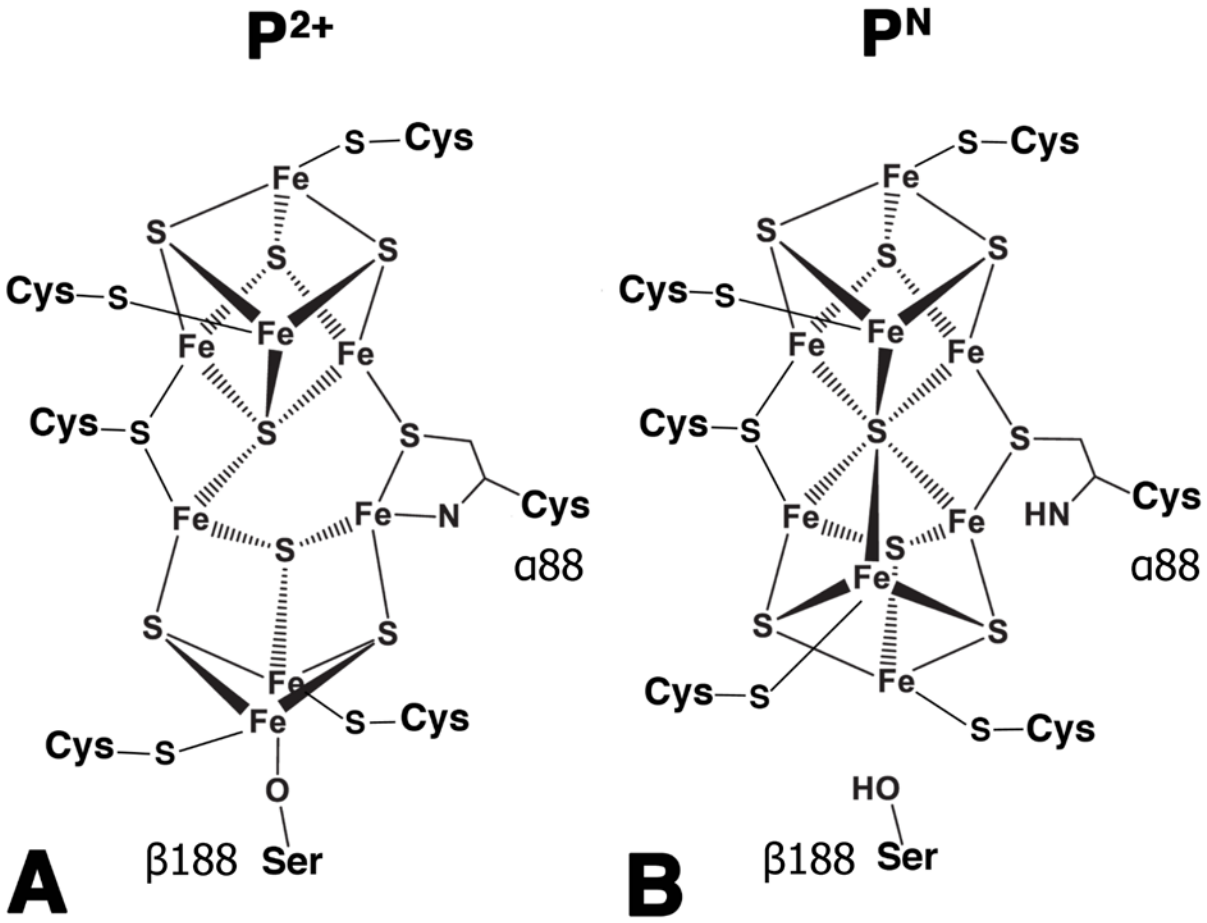

Figure 1. Presumed structural representations of the P^{2+} (A) and P^{N} (B) redox states of the P-cluster, highlighting differences in ligation.

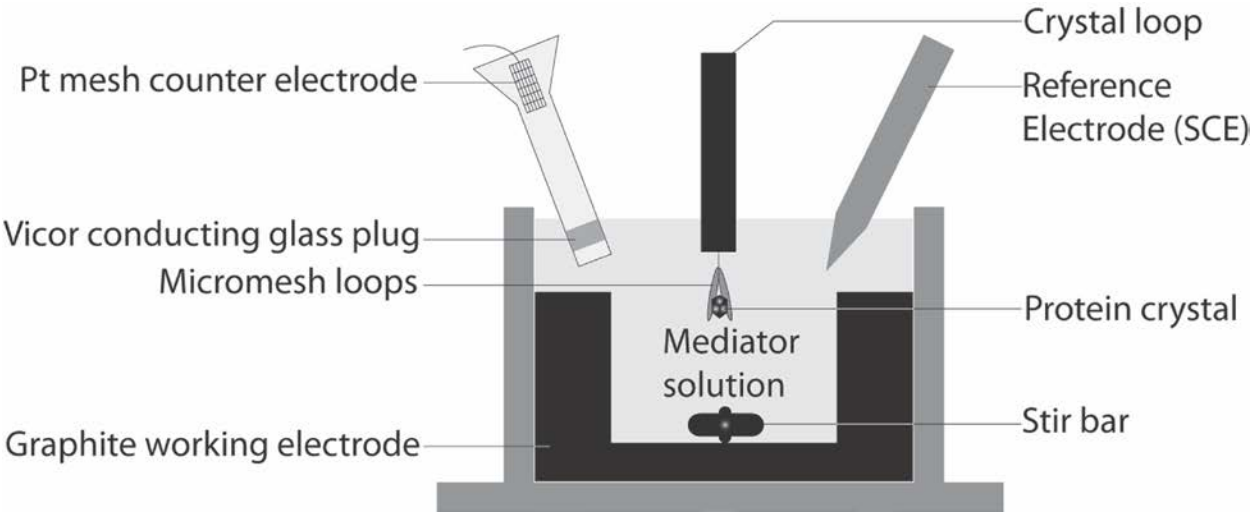

Figure 2. Schematic diagram of the crystal potential poising apparatus. Crystals were submerged in a stirred solution held at constant potential for 1 hour prior to flash cooling in liquid nitrogen to poise them in distinct structural states.

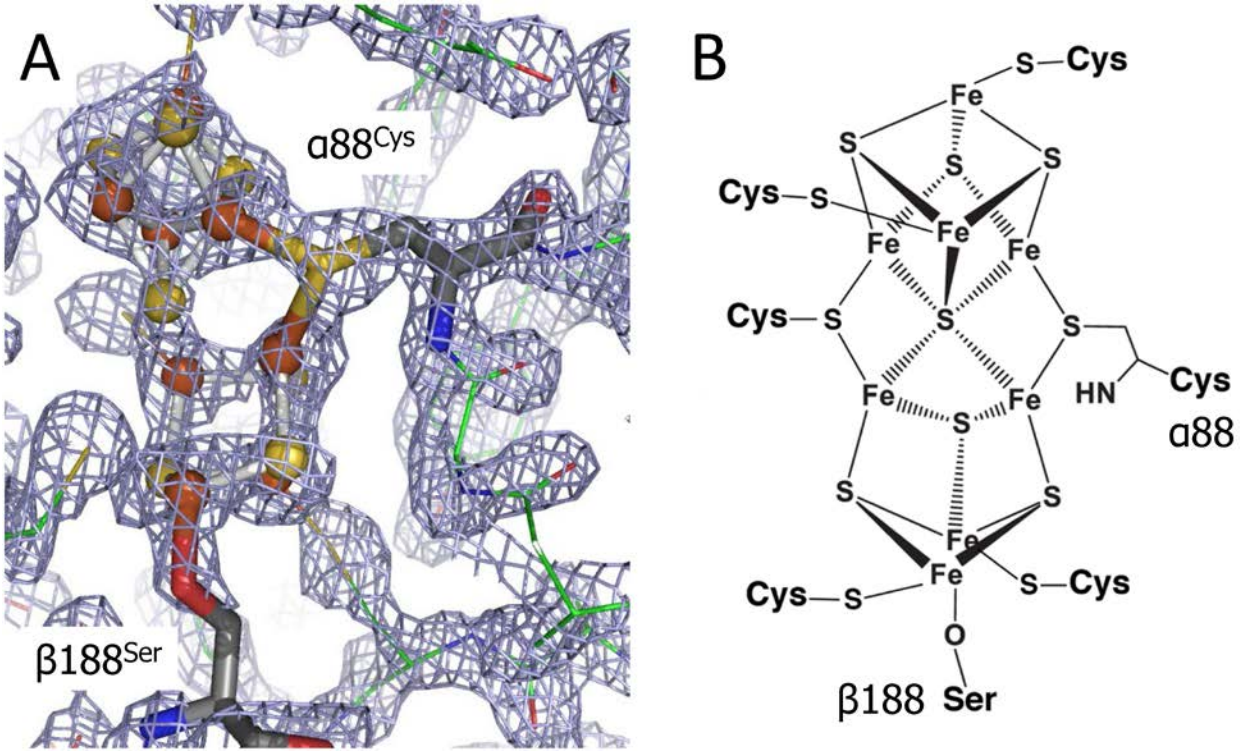

Figure 3. (A) Feature-enhanced electron density map (FEM) calculated using phinex.fem is showing P cluster in P^{+1} state. P cluster is shown in stick and balls, α-88^{Cys} and β-188^{Ser} are shown in sticks, and MoFe protein is shown in lines. FEM is contoured to 1.5 σ. (B) Structural representation of the P^{1+} redox state of the nitrogenase P-cluster deduced from the present studies.

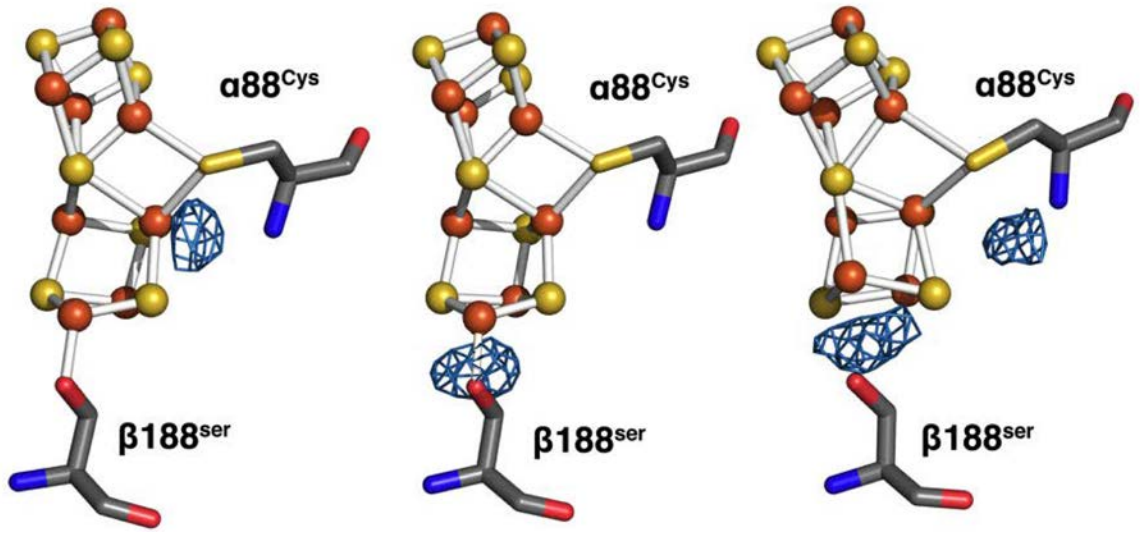

Figure 4. *Fo-Fc* difference electron density analysis of electrochemically poised P-cluster structures. The P^{1+} model is shown (A) with *Fo-Fc* (P^{1+}-P^{2+}) difference electron density contoured to 5σ. The P^{1+} model is shown (B) with *Fo-Fc* (P^{1+}-P^{N}) difference electron density contoured to 2σ (peak still clearly present at 3σ). The PN model (C) with *Fo-Fc* (P^{N}-P^{2+}) difference electron density contoured to 3σ highlighting the differences between the two-electron reduced and oxidized poised structures.

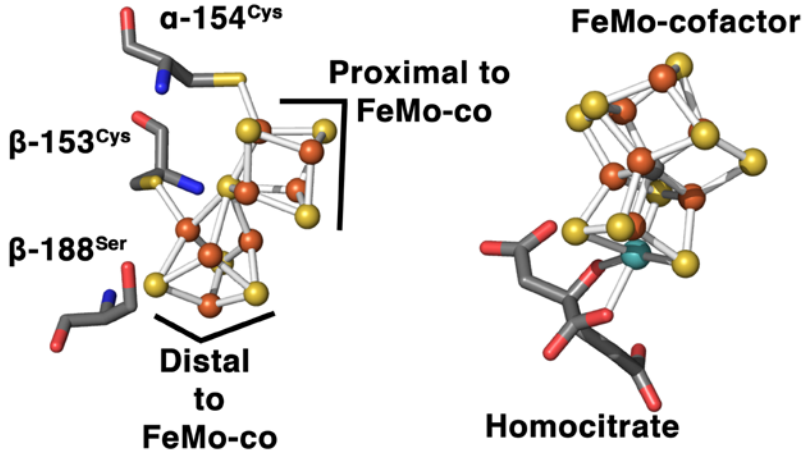

Figure 5. Ball and stick representations of the P-cluster and FeMo-cofactor, highlighting the orientation of the P-cluster cubanes with respect to the FeMo-cofactor.

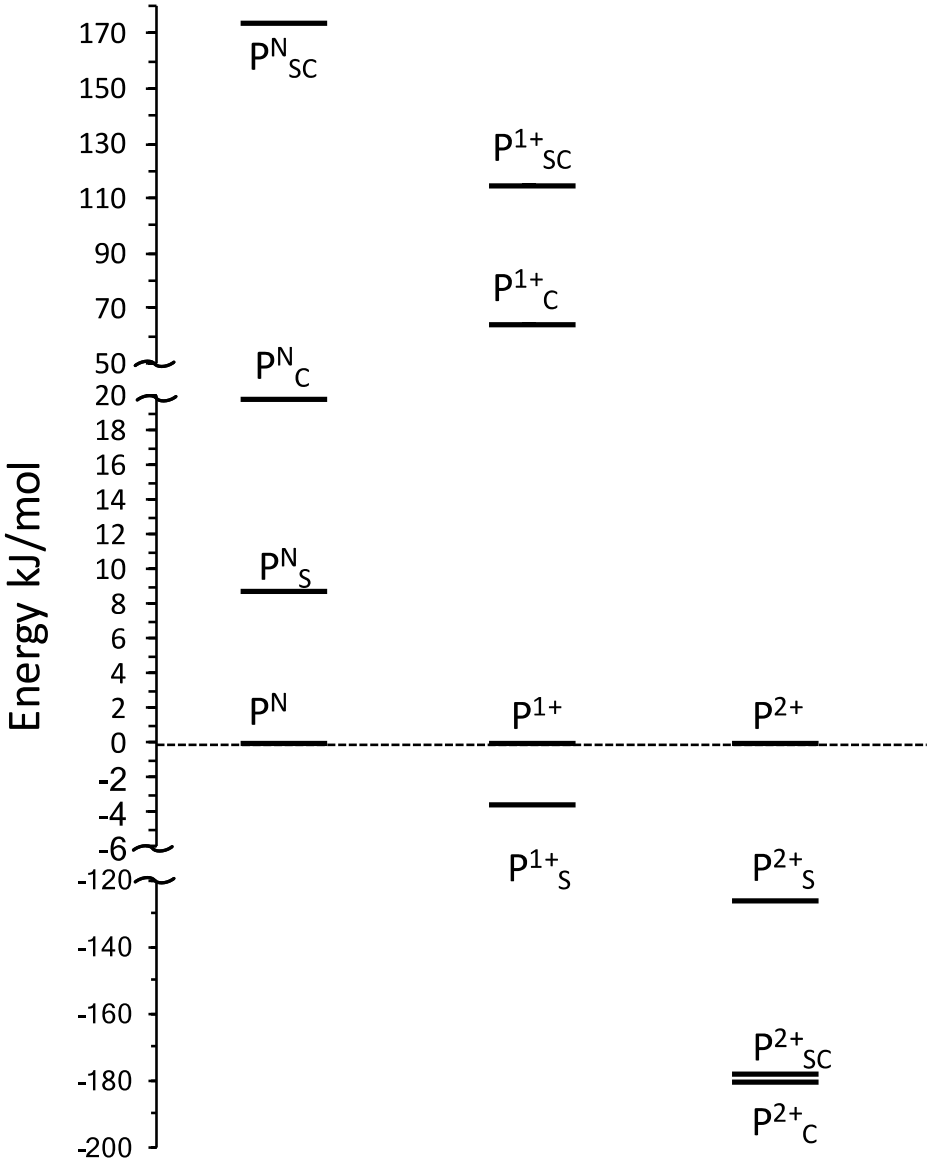

Figure 6. Free energy ordering of the possible ligation forms of the P-cluster in the P^N, P^{1+}, and P^{2+} states. The subscripts 'S' and 'C' indicate Ser and Cys bound P-cluster, respectively. For each state, all of the energy are relative to the non-ligated cluster. Note the change of the energy scale axis that is adopted for clarity of visualization of all the various species in the same graph.

Structural characterization of the P^{1+} intermediate state of the P-cluster of nitrogenase

Stephen M Keable, Oleg A Zadvornyy, Lewis E Johnson, Bojana Ginovska, Andrew J Rasmussen, Karamatullah Danyal, Brian J Eilers, Gregory A Prussia, Axl X LeVan, Simone Raugei, Lance C. Seefeldt and John W. Peters

J. Biol. Chem. published online May 2, 2018
